Comprehensive analysis of new prognostic signature based on ferroptosis-related genes in clear cell renal cell carcinoma

Bin Zheng[1,2,3,*], Zhihong Niu[1,2,3,*], Shubin Si[4], Guiting Zhao[2,3], Jianwei Wang[5], Zhongshun Yao [2,3], Fajuan Cheng[6,7], Wei He[2,3]

[1]Cheeloo College of Medicine, Shandong University, Jinan, Shandong, China
[2]Department of Urology, Shandong Provincial Hospital Affiliated to Shandong First Medical University, Jinan, Shandong, China
[3]Department of Urology, Shandong Provincial Hospital Affiliated to Shandong University, Jinan, Shandong, China
[4]Department of Urology, People's Hospital of Yiyuan County, Zibo, Shandong, China
[5]Department of Urology, Shandong Provincial ENT Hospital Affiliated to Shandong University, Jinan, Shandong, China
[6]Department of Nephrology, Shandong Provincial Hospital Affiliated to Shandong University, Jinan, Shandong, China
[7]Department of Nephrology, Shandong Provincial Hospital, Cheeloo College of Medicine, Shandong University, Jinan, Shandong, China
*Equal contribution

Correspondence to: Fajuan Cheng, Wei He; email: chengfajuan@bjmu.edu.cn, hewei@bjmu.edu.cn

ABSTRACT

Clear cell renal cell carcinoma (ccRCC) is an aggressive tumor and the most common subtype of RCC. Ferroptosis is a novel form of regulated cell death, and ferroptosis-related genes (FRGs) have been associated with the prognosis of patients with certain cancers. However, the detailed prognostic correlation between FRGs and ccRCC has not yet been elucidated. To address this, the current study used The Cancer Genome Atlas (TCGA) dataset to explore 64 FRGs and determine their prognostic value in ccRCC. Results showed that 52 out of the 64 genes displayed significantly different expression levels in tumor tissue, and 35 out of the 52 differentially expressed genes (DEGs) were associated with overall survival. Subsequently, a four-gene prognostic signature (*CD44*, *DPP4*, *NCOA4* and *SLC7A11*) was constructed and could successfully distinguish ccRCC patients with different prognosis in TCGA train and test sets. Furthermore, clinical ccRCC samples from our medical center were used to verify the application value of the new prognostic signature through immunohistochemistry and quantitative real-time polymerase chain reaction (qRT-PCR). Biological functional analysis implied that immune-related functions and pathways were enriched in the TCGA cohort and the immune status scores were significantly different between high- and low-risk sets. These results suggest that the four ferroptosis-related regulatory genes can act as reliable prognostic biomarkers of ccRCC, and might be exploited as potential targets of therapeutic strategies.

INTRODUCTION

Kidney or renal cancer is the 6 most common malignant cancer in males and the 8 most common in females. There will be 73,820 patients of renal cancer diagnosed in the United States, of which 14,770 patients succumbed from the disease [1]. Among the various histological types of kidney cancer, RCC is the most common type, accounting for about 85% of all cases [2]. RCCs arise from nephrons, but there are distinct

histological subtypes of RCC that differ both in biology and survival outcomes. Clear cell RCC (ccRCC) is the most common subtype (70%-80% of all RCC cases) and is also one of the most aggressive subtypes [3]. Numerous treatments for ccRCC are available, including radical nephrectomy, nephron-sparing surgery, and immunotherapy, etc., but the overall prognosis has remained limited and immune-related adverse events remain to be improved [4–6]. Therefore, this calls for exploration and construction of potential prognostic models with the overarching goal of providing ccRCC patients with optimal treatments.

Previous studies confirmed that ccRCC is strongly associated with alterations in the von Hippel-Lindau (*VHL*) gene [7, 8]. Furthermore, several miRNAs (such as miR-99a, miR-106a, and miR203, etc.) and pathways (such as PI3K/AKT/mTOR, Wnt-β, and Hippo) modulate the process of ccRCC [9, 10]. In recent years, several studies have reported that ferroptosis may participate in a ccRCC-associated mechanism [11].

Ferroptosis was first introduced in 2012 by Dixon et al. [12]. As a ROS- and iron-dependent form of regulated cell death (RCD), ferroptosis is distinct from other RCDs (such as apoptosis, necroptosis, and autophagy) in both morphological changes and biochemical processes [13]. Studies have proven that diverse molecules, including *GPX4, SLC7A11* and *VDAC2/3*, regulate ferroptosis through affecting iron metabolism and lipid peroxidation [14–16]. Furthermore, recent data demonstrated that FRGs are closely associated with the prognosis of patients with hepatocellular carcinoma (HCC) [17]. However, it has not yet been elucidated whether FRGs are also associated with the prognosis of ccRCC patients.

Therefore, this study examined the expression pattern of 64 FRGs in ccRCC patients using data retrieved from TCGA database. Moreover, new risk stratification models were constructed, followed by validation of the prognostic value of the model using TCGA test cohort and clinical samples obtained from our medical center (the Shandong Provincial Hospital affiliated to Shandong First University). Finally, functional analysis was conducted to elucidate the potential mechanisms in ccRCC.

RESULTS

The expression pattern and correlation of ferroptosis genes in ccRCC

A heatmap was generated to analyze the expression pattern of FRGs in ccRCC. Most of the genes (52/64, 81.3%) showed a significantly different expression

level in the ccRCC tissues compared to the normal tissues (Figure 1A). Furthermore, univariate Cox analysis revealed that 35 out of the 52 DEGs were significantly associated with OS (Figure 1B). Next, a Venn diagram was constructed to screen out the prognostic ferroptosis-related DEGs, with results showing that 27 DEGs were associated with prognosis (Figure 1C). Finally, the 27 prognostic FRGs were preserved ($p < 0.05$, Figure 1D, 1E).

Moreover, correlation analysis was used to investigate the interactions among all selected genes, with results suggesting that most of the FRGs had a positive correlation (Figure 1F). The PPI network indicated that *SLC7A11*, *GCLM,* and *NFE2L2* were the hub genes (Figure 1G).

Construction of prognostic signature in the TCGA cohort

The entire TCGA cohort was randomly divided into train set ($n = 264$) and test set ($n = 261$) using the "caret" package. The 27 DEGs mentioned above were then measured as predictive genes and exposed to LASSO analysis. From the results, six FRGs were screened out based on the optimal value of λ (Supplementary Figure 1A, 1B). Subsequently, multivariate Cox analysis was performed, and a four genes prognostic model was finally constructed (Figure 2A). The risk score was then determined using the coefficients and expression level of each gene: risk score = $(0.015) \times CD44 + (-0.005) \times DPP4 + (-0.017) \times NCOA4 + (0.432) \times SLC7A11$. According to the median risk score, patients in the train set were grouped into high- and low risk sets, and followed by comparison of the OS using the K-M curve. Results showed that ccRCC patients in the high-risk group had a poorer OS compared to patients in the low-risk group (Figure 2B). The distribution of the four FRGs signature based on risk scores is also displayed in Figure 2C, 2D, which was consistent with results of the K-M curve. Furthermore, time-dependent ROC analysis demonstrated that the prognostic signature had an advanced predictive performance for OS, with AUC values equal to 0.756, 0.753 and 0.769 at one, two and three years, respectively (Figure 2E). Finally, PCA and t-SNE analyses revealed that the two groups of patients were distributed in two different directions (Figure 2F, 2G).

Validation of the four-gene signature

According to the median risk score from train group, patients in test group were also categorized into high- and low-risk. Results showed that the survival outcome of high-risk patients was worse than that of low-risk patients, which was consistent with results of the train
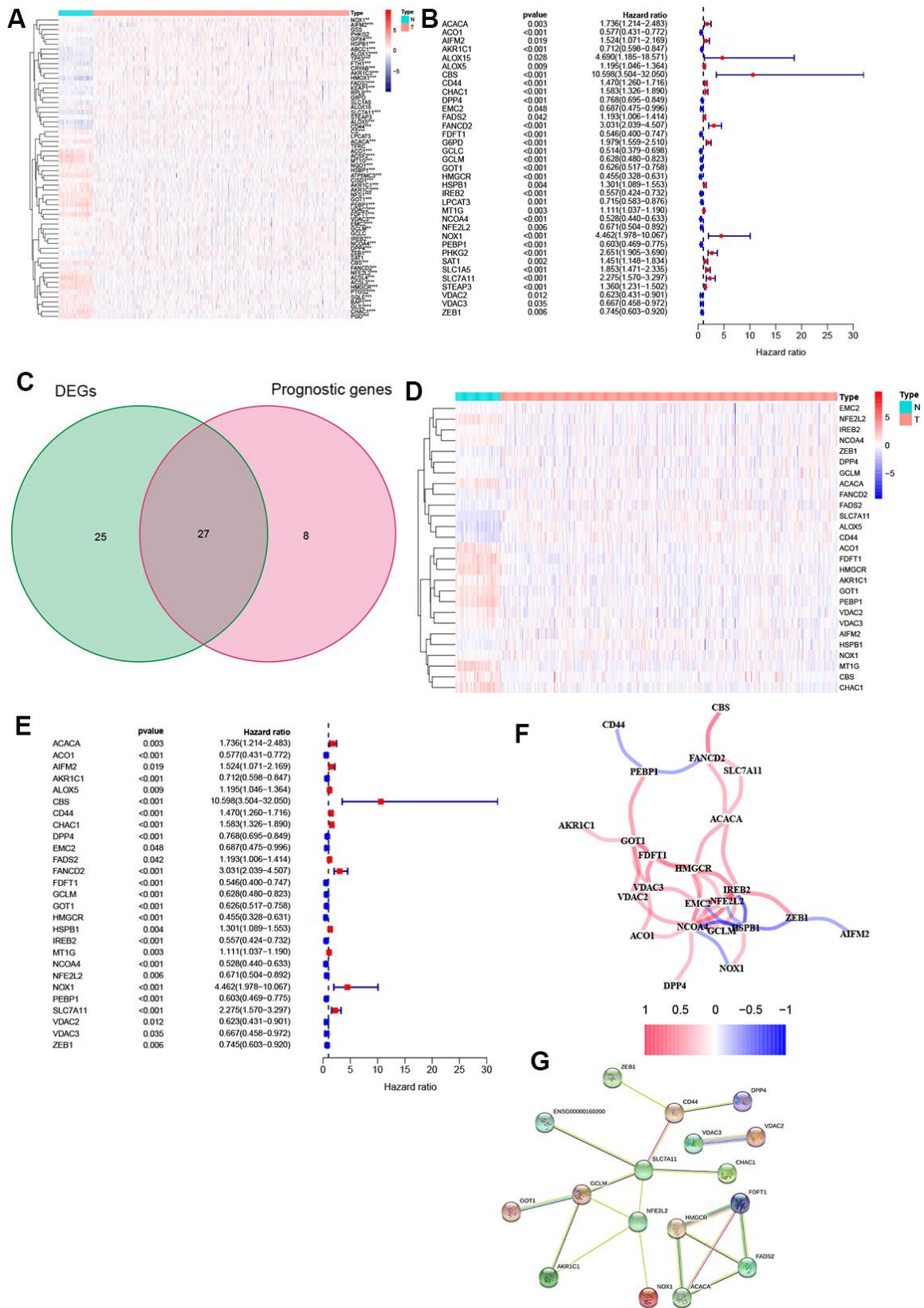
Figure 1. Identification of FRGs. (**A**) 52 genes showed significant differences in expression in ccRCC tissue. (**B**) 35 of the DEGs were associated with OS in univariate Cox analysis. (**C**) Venn plot to identify prognostic DEGs. (**D**) 27 overlapping genes show significantly different levels of expression in ccRCC tissues. (**E**) Forest plot displaying result of univariate Cox analysis between prognostic DEGS and OS. (**F**) The correlation network of prognostic DEGs. (**G**) The PPI network from the STRING database. *, *P* < 0.05; **, *P* < 0.01; ***, *P* < 0.001.

set (Figure 3A). The distribution of risk scores confirms that patients with high-risk scores have poorer survival outcomes compared to patients with low-risk scores (Figure 3B, 3C). The ROC curve demonstrated that the four-gene signature had a preferable predictive capacity for OS, with AUC values of 0.718, 0.644 and 0.670 at one, two and three years, respectively (Figure 3D). In addition, PCA and t-SNE analyses confirmed that the two groups of patients with ccRCC were dispensed in two directions (Figure 3E, 3F).
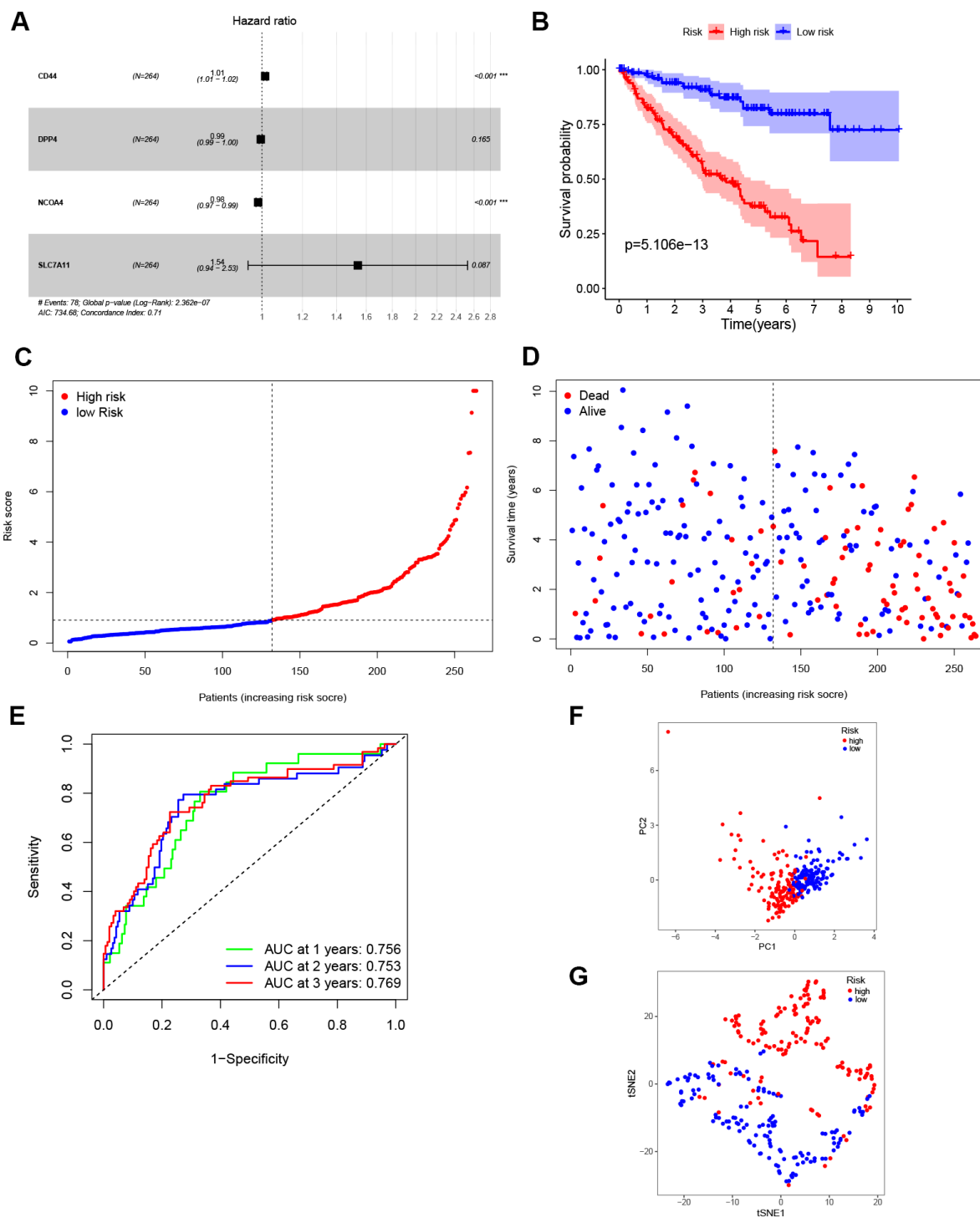

Figure 2. Construction of the prognostic model. (**A**) Construction of multivariate Cox analysis prognostic model. (**B**) K-M curve for the OS of ccRCC patients in high- and low-risk sets in the train set. (**C**, **D**) Distribution of risk scores and corresponding OS status in the train set. (**E**) ROC curve of the prognostic signature in the train set. (**F**, **G**) PCA and t-SNE analyses of the TCGA train set.

Furthermore, the robustness of the four-gene model was verified for its clinical application using KIRC samples obtained from our medical center. IHC images showed that the normal renal tissue had weak staining for *CD44*, *DPP4* and *SLC7A11* in the cytoplasm and cell membrane, while *NCOA4* displayed the opposite trend in normal tissues (Figure 4A, 4C, 4E). On the other hand, moderate and strong staining patterns for *CD44*, *DPP4*, and *SLC7A11* were observed in the cytoplasm and cell membrane of tumor tissues (Figure 4B, 4D, 4F), while *NCOA4* only exhibited weak positive staining on the cell membrane of tumor tissues (Figure 4G, 4H). These unique IHC staining patterns illustrate that the four genes can be used to predict clinical outcome and can distinguish cancerous tissue from normal tissue.
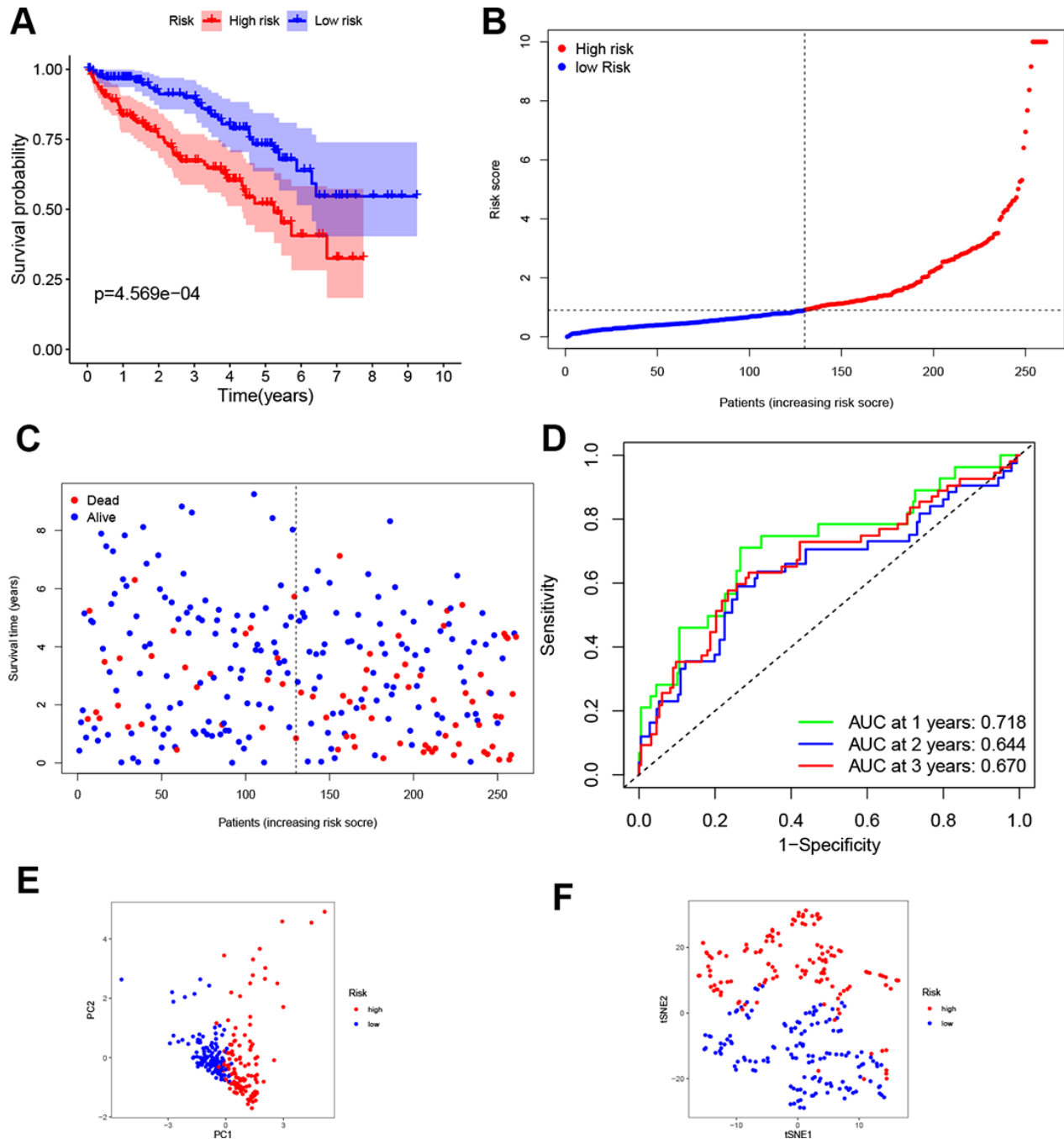

Figure 3. Validation of the four-gene signature. (**A**) K-M curve for the OS of ccRCC patients in the test set. (**B**, **C**) Distribution of the risk scores and corresponding OS status in test set. (**D**) ROC curve of the prognostic signature in test set. (**E**, **F**) PCA and t-SNE analyses of the TCGA test set.

Subsequent qRT-PCR analysis also showed that the expression level of *CD44*, *DPP4* and *SLC7A11* in ccRCC samples are significantly higher than that in paired non-tumor samples (Figure 4I). In addition, the expression level of *NCOA4* in ccRCC samples is lower than that in paired non-tumor samples ($p < 0.05$, Figure 4I).

Independent prognostic value of the constructed signature in ccRCC

To determine whether the four-gene signature could serve as independent prognostic factor, univariate and multivariate Cox regression analyses were operated on both the train and test sets. Univariate Cox analysis indicated that age, tumor grade, tumor stage and risk score were associated with OS in both train and test sets ($p < 0.05$, Figure 5A, 5C). The variables with associated *P* value <0.1 were then enlisted into the multivariate Cox analysis, which showed that the predictors were risk score and tumor stage in both train and test sets ($p < 0.05$, Figure 5B, 5D).

Functional analyses

To illustrate the biological functions and pathways of genes that were differentially expressed in ccRCC tissues compared with non-cancerous tissues, GO enrichment and KEGG pathway analyses were conducted. GO analysis suggested that the DEGs were enriched in peptidase regulator activity, signaling receptor activator activity, receptor ligand activity, and plasma membrane (FDR < 0.05, Figure 6A), which is consistent with previous studies [18–21]. On the other hand, KEGG

pathway analyses implied that the DEGs were enriched in the TNF signaling pathway, PPAR signaling pathway, p53 signaling pathway, folate biosynthesis, bile secretion, and cholesterol metabolism (Figure 6B), which is congruent with preceding studies [22–27]. However, the DEGs were also enriched in several immune functions and immune-associated pathways, such as cytokine-cytokine receptor interaction, lymphocyte mediated immunity, and complement activation, complement and coagulation cascades (FDR < 0.05, Figure 6A, 6B).

Considering the association between different DEGs and immune status, we further explored the interaction between risk score and immune status in the TCGA cohort. Major immune cells and functions were quantified with enrichment scores using ssGSEA. Results indicated that the scores of antigen-presenting cells (APC) and functions in the high-risk group, including DCs, iDCs and APC co-inhibition, were higher than in the low-risk group ($p < 0.05$, Figure 6C, 6D). However, the score of aDCs was lower in the high-risk group. Notably, cellular immunity, especially T cell-related immune cells and functions, including CD8+ T cell, Th1 cell, Th2 cell, Tfh cell and T cell co-stimulation, had higher scores in the high-risk group ($p < 0.05$, Figure 6C, 6D). Furthermore, consistent with the KEGG analysis, quantification of cytokine-cytokine receptor (CCR) interaction produced higher scores in the high-risk set ($p < 0.05$, Figure 6D). In addition, tumor infiltrating lymphocytes (TIL), the function of checkpoint regulators, and the ability of inflammation-promoting molecules displayed elevated scores in the high-risk group ($p < 0.05$, Figure 6C, 6D).
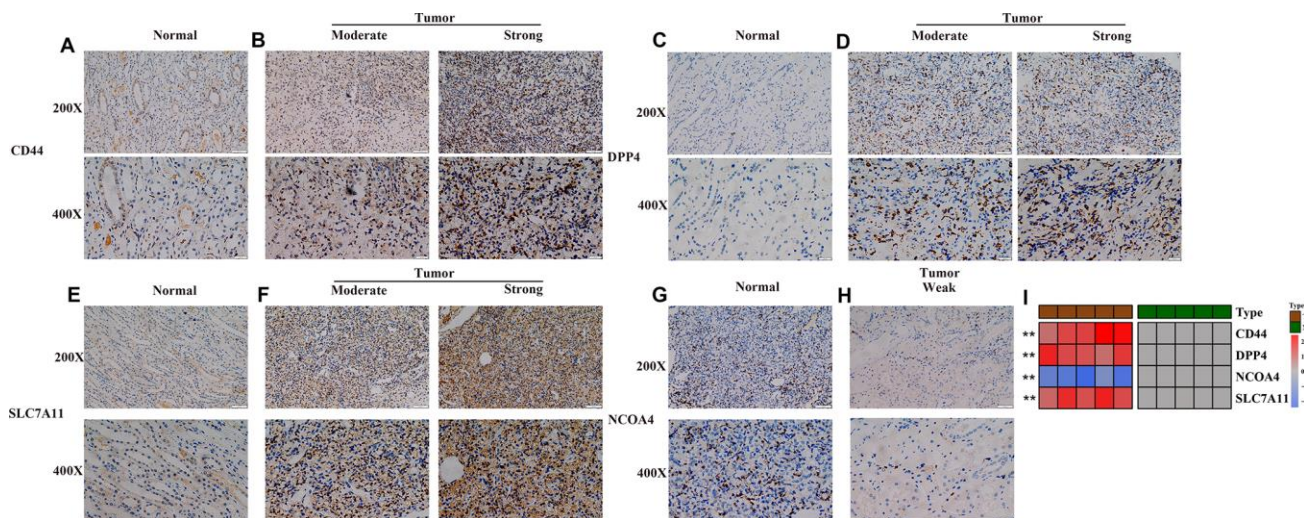

Figure 4. Experimental verification of four genes in the prognostic signature. (**A**–**H**) Immunohistochemical images of expression of the four proteins from the prognostic signature in non-tumor tissue samples (**A**, **C**, **E**, **G**) and tumor samples (**B**, **D**, **F**, **H**). (**I**) mRNA expression levels of 4 ferroptosis-related genes were evaluated using qRT–PCR in ccRCC samples and normal samples. *, $P < 0.05$; **, $P < 0.01$; ***, $P < 0.001$.

Finally, we performed co-expression analysis between four ferroptosis genes through Person's correlation analysis. As shown in Supplementary Figure 2, based on the optimal correlation, we selected *NCOA4* and *SLC7A11* as the hub genes. Then, GSEA analysis was conducted to explore the underlying mechanisms based on the TCGA data. Notably, the results showed that overexpression of *NCOA4* was associated with renal cell carcinoma, the JAK-STAT pathway, Toll-like pathway and the NOD-like receptor pathway (|NES|> 1, $p < 0.05$, FDR < 0.25, Supplementary Figure 3A–3D). In addition, overexpressed SLC7A11 enriched in cell cycle and NOD-like receptor pathway as well (|NES|> 1, $p < 0.05$, FDR < 0.25, Supplementary Figure 3E, 3F).

DISCUSSION

Several recent studies have recently confirmed that ferroptosis, a novel recognized form of RCD, occurs due to accumulation of lethal lipid peroxidation. Morphologically, ferroptosis is characterized by small mitochondria, reduced mitochondria crista, and ruptured outer mitochondrial membrane [28]. Emerging evidence has indicated that several compounds, such as

sulfasalazine and sorafenib induce ferroptosis in cancer cells [29]. Many studies have also reported that dysregulated ferroptosis may affect multiple pathological processes, such as cancer cell death, renal failure, and T cell immunity [14, 15, 30]. Therefore, considering the significant role of ferroptosis in regulating cell death, the exact role of this process in ccRCC should be investigated.

Here, major knowledge gaps have been identified, including evaluation of FRGs to assess prognostic value as well as the potential mechanisms in ccRCC. Firstly, the expression pattern of 64 ferroptosis-related regulator genes in ccRCC was explored, with results showing that 52 of these regulators were aberrantly expressed in ccRCC. Furthermore, 35 of the 52 DEGs were associated with the prognosis of ccRCC patients. Next, 27 prognostic ferroptosis-related DEGs were screened out by Venn diagram, and a prognostic model with four genes (*CD44*, *DPP4*, *NCOA4*, and *SLC7A11*) was developed via LASSO and multivariate Cox regression analyses. With the median risk score, patients were then grouped into low- and high-risk groups. The K-M curve and ROC curve indicated that this four-gene signature
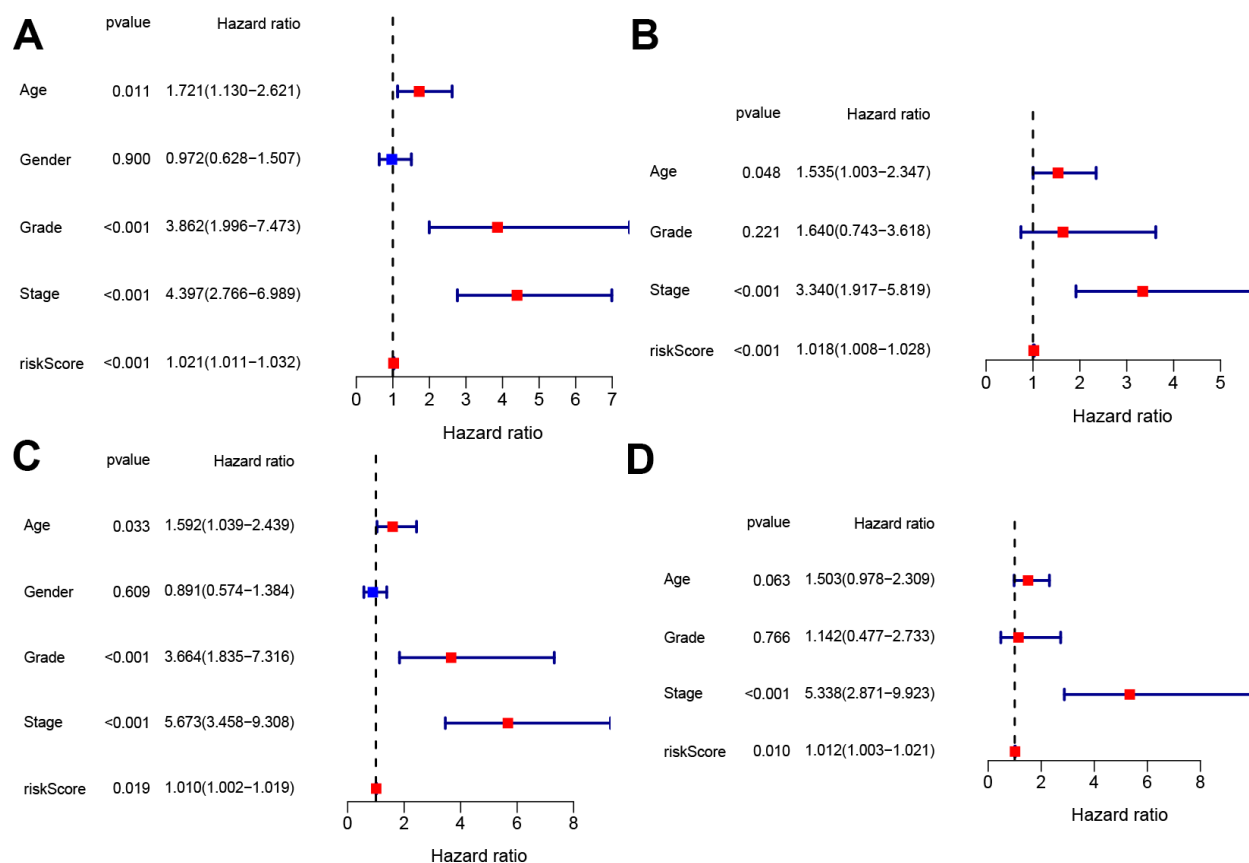

Figure 5. Independent prognostic value of the constructed signature. Univariate and multivariate Cox analyses regarding OS in the train set (**A**, **B**) and test set (**C**, **D**).

had a good ability to predict prognosis. In addition, multivariate Cox analysis showed that the risk score was an independent prognostic factor. Besides, the prognostic signature was validated using the test set and in KIRC samples from our hospital, with results further suggesting the prognostic value of the four-gene signature in clinical application. Finally, GO and KEGG enrichment analyses were performed in the TCGA cohort. In addition to the ferroptosis-related functions and pathways, several tumor immune-related functions and pathways were enriched. Moreover, ssGSEA results showed that the APCs scores and cellular immunity scores, especially those of T cell-related immune cells, were also higher in the high-risk group than in the low-risk group. It has been proposed that ferroptotic cells may release diverse 'find me' signaling molecules, which could attract APCs or other immune cells to the location of ferroptotically dying cells [11]. Furthermore, T cell immunity, especially CD8+ T cells could promote ferroptosis-specific lipid peroxidation in tumor cells, thereby contributing to the antitumor efficacy of immunotherapy [31]. Therefore, the prognostic models established in this study have the potential to evaluate

the prognosis of ccRCC patients. Meanwhile, the four selected ferroptosis-related regulatory genes can be exploited as potential targets of therapeutic strategies and the relevant mechanisms should be explored further.

Specifically, the four genes in the prognostic signature perform distinct functions in the process of ferroptosis. For example, *NCOA4* plays important role in regulating iron metabolism. Several studies reported that knocking down these genes suppressed erastin-induced ferroptosis and/or amino acid/cystine deprivation-induced ferroptosis [32, 33]. In addition, *DPP4* inhibited erastin-induced ferroptosis in colorectal cancer after its activity was blocked by *p53*. However, in the absence of *p53*, *DPP4* combines with *NOX1* to form the *NOX-DPP4* complex, thereby leading to plasma membrane lipid peroxidation and ferroptosis [21, 34]. *SLC7A11* participates in many ferroptosis-related signaling pathways. Studies have reported that *BAP1* could promote ferroptosis by blocking the expression of *SLC7A11*. Moreover, *SLC7A11* could induce ferroptosis when the African-restricted polymorphism S47 in the *p53* (*p53^{3KR}*) gene was mutated [26, 35]. *CD44*, a marker of cancer stem
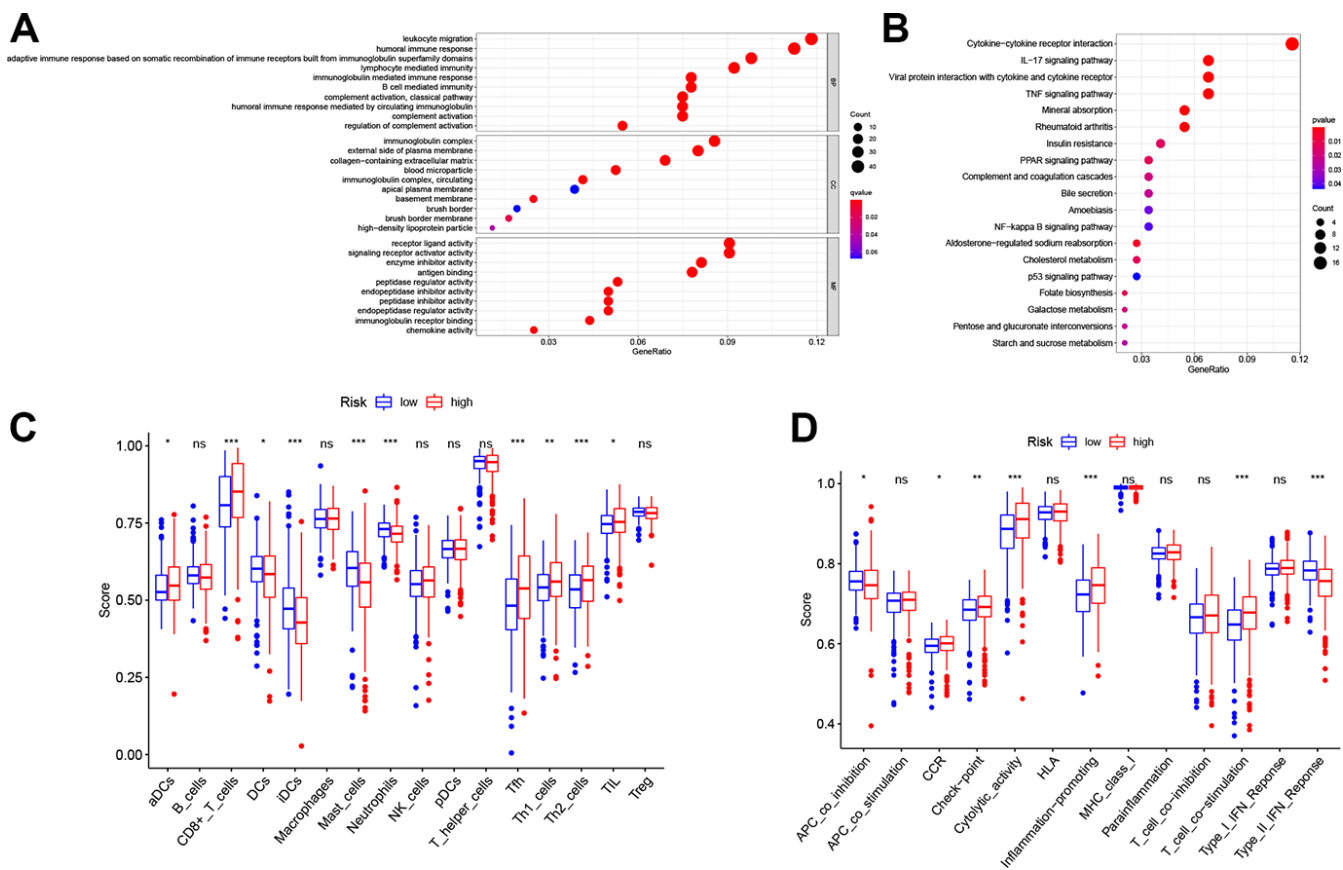

Figure 6. Functional analyses in the TCGA cohort. Representative results of the most significant GO enrichment (A) and KEGG pathways (B) in the TCGA cohort. ssGSEA scores of immune cells (C) and immune-related functions (D) between different risk groups. ns, not significant; *, $P < 0.05$; **, $P < 0.01$; ***, $P < 0.001$.

cells, has also been shown to regulate iron homeostasis and modulate iron entry into tumor cells [36]. In particular, *CD44v*, the isoform of *CD44*, could stabilize protein xCT and hence stimulate glutathione synthesis, which then further undermined ROS-induced stress signaling, a ferroptosis hallmark [37]. However, despite these observations, there are only limited studies concerning the mechanism of ferroptosis in ccRCC. Therefore, additional experimental proof about these ferroptosis-related regulators in ccRCC is needed.

There are several limitations in this current study. Firstly, the ccRCC cohort is relatively small and clinical data of the samples is not complete. Secondly, the lack of *in vitro* experimental verification affects the rigor of this study. Although we conducted GO and KEGG analysis, the specific upstream and downstream target molecules as well as the specific regulatory mechanisms still need to be verified. Therefore, future studies should include the prospective data of ccRCC patients and *in vitro* experimental verification in order to strengthen the findings of this study. Overall, this research is far from being completed and most likely this process will continue in the next years. Given the limited knowledge of ferroptosis-related genes, it is of critical urgency to interrogate detailed mechanism and novel targets for future clinical application.

Collectively, the finding of this study illustrated a dysregulated expression profile of FRGs between ccRCC and normal samples. Many clinicopathological features, including patients' age, tumor grade and stage could act as independent prognostic factors, which illustrated the pivotal role of these genes in the development of ccRCC. Finally, a four-gene prognostic model was constructed to determine various prognoses of ccRCC patients, and the model implied that *CD44*, *DPP4*, *NCOA4*, and *SLC7A11* may serve as potential molecular biomarkers of ccRCC.

MATERIALS AND METHODS

Data collection

Expression data and clinical information of 539 ccRCC and 72 normal patients were obtained from the TCGA database (https://portal.gdc.cancer.gov/). Expression data were normalized by "limma" package. After performing a comprehensive literature review, 64 FRGs were identified [13, 19, 38–41] (Supplementary Table 1).

Selection of intersected genes between differential expression- and prognostic ferroptosis-related genes

DEGs in paired tumor and non-tumor tissues were assessed by "limma" package. Univariate Cox analysis

of overall survival (OS) was then conducted to obtain prognostic genes. Finally, intersected FRGs were screen out using the "venn" R package. The differential expression patterns, co-expression correlation analysis, and prognostic values were visualized by "survival", "igraph" and "pheatmap" R package.

Construction and validation of the prognostic signatures

The TCGA cohort was randomly divided into two groups (train and test groups) by using the "caret" package. Least absolute shrinkage and selection operator (LASSO) Cox regression analysis was conducted in train set with the "glmnet" R package. Multivariate cox analysis was performed to build prognostic models. The median value of risk scores was calculated to stratify ccRCC patients into high-risk and low-risk sets by the following formula: $\text{Risk score} = \sum_{1}^{n} Coef_n \times x_n$ (where $Coef_n$ is the coefficient and x_n is the expression level of each intersected gene). Next, a Kaplan-Meier (K–M) curve was used to analyze the OS in train and test groups, respectively. Receiver operating characteristic (ROC) analysis was also executed to assess the prediction efficiency of prognosis. Based on the expression profile of four FRGs, PCA and t-SNE analysis were performed to demonstrate the expression patterns of various FRGs in diverse groups. Finally, IHC pattern was certified by utilizing KIRC clinical samples from our hospital. Univariate and multivariate Cox analyses were utilized to investigate independent prognostic factors for ccRCC patients.

Functional analyses

A protein–protein interaction (PPI) network was built for prognostic DEGs by the STRING database (http://string-db.org/). Gene Ontology (GO) and Kyoto Encyclopedia of Genes and Genomes (KEGG) analyses based on the DEGs were then operated by utilizing "clusterProfiler" package. In addition, the score of major immune cells and immune-related pathways were determined with single-sample gene set enrichment analysis (ssGSEA). GSEA was performed using GSEA v4.1.0 (http://www.broadinstitute.org/gsea/).

Immunohistochemistry

Ten pairs of ccRCC and adjacent normal tissues were collected from Shandong provincial Hospital affiliated to Shandong First University during January 2021 to February 2021. The experiment was approved by the Shandong Provincial Hospital Ethics Committee (Approval number: SWYX: NO.2021-118) and written

informed consents were signed by each patient before the study began. IHC was performed according to previously described standard procedures [42]. All samples were incubated with rabbit polyclonal antiCD44 (ab189524), antiNCOA4 (ab62495), antiDPP4 (ab187048) and antiSLC7A11 (ab175186) antibodies overnight at 4° C and were then washed. Two pathologists independently assessed the IHC slides.

RNA analysis, extraction, and quantitative real-time PCR

Total RNA of frozen tissue was extracted by TRIzol reagent (Tiangen Biotech (Beijing)), and 1 μg of total RNA was reverse transcribed using the FastKing RT Kit (Tiangen Biotech (Beijing)) according to the manufacturer's instructions. Followed by measuring with a real-time quantitative PCR system. The primers used in this study were provided by Beijing Dingguo Changsheng Company and are shown in Supplementary Table 2. The expression data was log2 transformed: $\log2(\exp + 0.01)$.

Statistical analysis

Mann-Whitney tests were utilized to measure gene expression between ccRCC and non-tumor tissues. Associated samples with incomplete clinical information were eliminated. All data analyses were conducted using the R statistical package (R version 4.0.1). A two-tailed $p < 0.05$ was considered statistically significant.

Data availability statement

The data used to support the findings of this study are available from the corresponding author upon request.

AUTHOR CONTRIBUTIONS

Conceptualization: B.Z, W.H, G.T.Z; Methodology: B.Z, Z.H.N, J.W.W, Y.S.Y, S.B.S; Writing - original draft preparation: B.Z, F.J.C; Writing - review and editing: Z.H.N, W.H; Supervision: Z.H.N, W.H.

CONFLICTS OF INTEREST

The authors declare that they have no conflicts of interest.

REFERENCES

1. Siegel RL, Miller KD, Jemal A. Cancer statistics, 2019. CA Cancer J Clin. 2019; 69:7–34.
https://doi.org/10.3322/caac.21551
PMID:30620402

2. Barata PC, Rini BI. Treatment of renal cell carcinoma: Current status and future directions. CA Cancer J Clin. 2017; 67:507–24.
https://doi.org/10.3322/caac.21411
PMID:28961310

3. Vuong L, Kotecha RR, Voss MH, Hakimi AA. Tumor Microenvironment Dynamics in Clear-Cell Renal Cell Carcinoma. Cancer Discov. 2019; 9:1349–57.
https://doi.org/10.1158/2159-8290.CD-19-0499
PMID:31527133

4. Choueiri TK, Motzer RJ. Systemic Therapy for Metastatic Renal-Cell Carcinoma. N Engl J Med. 2017; 376:354–66.
https://doi.org/10.1056/NEJMra1601333
PMID:28121507

5. Rizzo A, Mollica V, Santoni M, Ricci AD, Rosellini M, Marchetti A, Montironi R, Ardizzoni A, Massari F. Impact of Clinicopathological Features on Survival in Patients Treated with First-line Immune Checkpoint Inhibitors Plus Tyrosine Kinase Inhibitors for Renal Cell Carcinoma: A Meta-analysis of Randomized Clinical Trials. Eur Urol Focus. 2021. [Epub ahead of print].
https://doi.org/10.1016/j.euf.2021.03.001
PMID:33714725

6. Massari F, Mollica V, Rizzo A, Cosmai L, Rizzo M, Porta C. Safety evaluation of immune-based combinations in patients with advanced renal cell carcinoma: a systematic review and meta-analysis. Expert Opin Drug Saf. 2020; 19:1329–38.
https://doi.org/10.1080/14740338.2020.1811226
PMID:32799582

7. Nickerson ML, Jaeger E, Shi Y, Durocher JA, Mahurkar S, Zaridze D, Matveev V, Janout V, Kollarova H, Bencko V, Navratilova M, Szeszenia-Dabrowska N, Mates D, et al. Improved identification of von Hippel-Lindau gene alterations in clear cell renal tumors. Clin Cancer Res. 2008; 14:4726–34.
https://doi.org/10.1158/1078-0432.CCR-07-4921
PMID:18676741

8. Brugarolas J. Molecular genetics of clear-cell renal cell carcinoma. J Clin Oncol. 2014; 32:1968–76.
https://doi.org/10.1200/JCO.2012.45.2003
PMID:24821879

9. Braga EA, Fridman MV, Loginov VI, Dmitriev AA, Morozov SG. Molecular Mechanisms in Clear Cell Renal Cell Carcinoma: Role of miRNAs and Hypermethylated miRNA Genes in Crucial Oncogenic Pathways and Processes. Front Genet. 2019; 10:320.
https://doi.org/10.3389/fgene.2019.00320
PMID:31110513

10. Yang WH, Ding CC, Sun T, Rupprecht G, Lin CC, Hsu D, Chi JT. The Hippo Pathway Effector TAZ Regulates Ferroptosis in Renal Cell Carcinoma. Cell Rep. 2019; 28:2501–08.e4.
https://doi.org/10.1016/j.celrep.2019.07.107
PMID:31484063

11. Friedmann Angeli JP, Krysko DV, Conrad M. Ferroptosis at the crossroads of cancer-acquired drug resistance and immune evasion. Nat Rev Cancer. 2019; 19:405–14.
https://doi.org/10.1038/s41568-019-0149-1
PMID:31101865

12. Dixon SJ. Ferroptosis: bug or feature? Immunol Rev. 2017; 277:150–57.
https://doi.org/10.1111/imr.12533
PMID:28462529

13. Xie Y, Hou W, Song X, Yu Y, Huang J, Sun X, Kang R, Tang D. Ferroptosis: process and function. Cell Death Differ. 2016; 23:369–79.
https://doi.org/10.1038/cdd.2015.158
PMID:26794443

14. Friedmann Angeli JP, Schneider M, Proneth B, Tyurina YY, Tyurin VA, Hammond VJ, Herbach N, Aichler M, Walch A, Eggenhofer E, Basavarajappa D, Rådmark O, Kobayashi S, et al. Inactivation of the ferroptosis regulator Gpx4 triggers acute renal failure in mice. Nat Cell Biol. 2014; 16:1180–91.
https://doi.org/10.1038/ncb3064 PMID:25402683

15. Yang WS, SriRamaratnam R, Welsch ME, Shimada K, Skouta R, Viswanathan VS, Cheah JH, Clemons PA, Shamji AF, Clish CB, Brown LM, Girotti AW, Cornish VW, et al. Regulation of ferroptotic cancer cell death by GPX4. Cell. 2014; 156:317–31.
https://doi.org/10.1016/j.cell.2013.12.010
PMID:24439385

16. Mou Y, Wang J, Wu J, He D, Zhang C, Duan C, Li B. Ferroptosis, a new form of cell death: opportunities and challenges in cancer. J Hematol Oncol. 2019; 12:34.
https://doi.org/10.1186/s13045-019-0720-y
PMID:30925886

17. Liang JY, Wang DS, Lin HC, Chen XX, Yang H, Zheng Y, Li YH. A Novel Ferroptosis-related Gene Signature for Overall Survival Prediction in Patients with Hepatocellular Carcinoma. Int J Biol Sci. 2020; 16:2430–41.
https://doi.org/10.7150/ijbs.45050 PMID:32760210

18. Dai E, Meng L, Kang R, Wang X, Tang D. ESCRT-III-dependent membrane repair blocks ferroptosis. Biochem Biophys Res Commun. 2020; 522:415–21.
https://doi.org/10.1016/j.bbrc.2019.11.110
PMID:31761326

19. Kajarabille N, Latunde-Dada GO. Programmed Cell-Death by Ferroptosis: Antioxidants as Mitigators. Int J Mol Sci. 2019; 20:4968.
https://doi.org/10.3390/ijms20194968
PMID:31597407

20. Kang R, Kroemer G, Tang D. The tumor suppressor protein p53 and the ferroptosis network. Free Radic Biol Med. 2019; 133:162–68.
https://doi.org/10.1016/j.freeradbiomed.2018.05.074
PMID:29800655

21. Xie Y, Zhu S, Song X, Sun X, Fan Y, Liu J, Zhong M, Yuan H, Zhang L, Billiar TR, Lotze MT, Zeh HJ 3rd, Kang R, et al. The Tumor Suppressor p53 Limits Ferroptosis by Blocking DPP4 Activity. Cell Rep. 2017; 20:1692–704.
https://doi.org/10.1016/j.celrep.2017.07.055
PMID:28813679

22. Venkatesh D, O'Brien NA, Zandkarimi F, Tong DR, Stokes ME, Dunn DE, Kengmana ES, Aron AT, Klein AM, Csuka JM, Moon SH, Conrad M, Chang CJ, et al. MDM2 and MDMX promote ferroptosis by PPARα-mediated lipid remodeling. Genes Dev. 2020; 34:526–43.
https://doi.org/10.1101/gad.334219.119
PMID:32079652

23. Martin-Sanchez D, Ruiz-Andres O, Poveda J, Carrasco S, Cannata-Ortiz P, Sanchez-Niño MD, Ruiz Ortega M, Egido J, Linkermann A, Ortiz A, Sanz AB. Ferroptosis, but Not Necroptosis, Is Important in Nephrotoxic Folic Acid-Induced AKI. J Am Soc Nephrol. 2017; 28:218–29.
https://doi.org/10.1681/ASN.2015121376
PMID:27352622

24. Han JY, Ahn KS, Baek WK, Suh SI, Kim YH, Kim TS, Kang KJ. Usefulness of bile as a biomarker via ferroptosis and cysteine prenylation in cholangiocarcinoma; role of diagnosis and differentiation from benign biliary disease. Surg Oncol. 2020; 34:174–81.
https://doi.org/10.1016/j.suronc.2020.04.019
PMID:32891325

25. Xu H, Zhou S, Tang Q, Xia H, Bi F. Cholesterol metabolism: New functions and therapeutic approaches in cancer. Biochim Biophys Acta Rev Cancer. 2020; 1874:188394.
https://doi.org/10.1016/j.bbcan.2020.188394
PMID:32698040

26. Jiang L, Kon N, Li T, Wang SJ, Su T, Hibshoosh H, Baer R, Gu W. Ferroptosis as a p53-mediated activity during tumour suppression. Nature. 2015; 520:57–62.
https://doi.org/10.1038/nature14344 PMID:25799988

27. Li X, Zhuang X, Qiao T. Role of ferroptosis in the process of acute radiation-induced lung injury in mice. Biochem Biophys Res Commun. 2019; 519:240–45.
https://doi.org/10.1016/j.bbrc.2019.08.165
PMID:31493867

28. Dixon SJ, Lemberg KM, Lamprecht MR, Skouta R, Zaitsev EM, Gleason CE, Patel DN, Bauer AJ, Cantley AM, Yang WS, Morrison B 3rd, Stockwell BR. Ferroptosis: an iron-dependent form of nonapoptotic cell death. Cell. 2012; 149:1060–72.
https://doi.org/10.1016/j.cell.2012.03.042
PMID:22632970

29. Dixon SJ, Patel DN, Welsch M, Skouta R, Lee ED, Hayano M, Thomas AG, Gleason CE, Tatonetti NP, Slusher BS, Stockwell BR. Pharmacological inhibition of cystine-glutamate exchange induces endoplasmic reticulum stress and ferroptosis. Elife. 2014; 3:e02523.
https://doi.org/10.7554/eLife.02523 PMID:24844246

30. Matsushita M, Freigang S, Schneider C, Conrad M, Bornkamm GW, Kopf M. T cell lipid peroxidation induces ferroptosis and prevents immunity to infection. J Exp Med. 2015; 212:555–68.
https://doi.org/10.1084/jem.20140857
PMID:25824823

31. Wang W, Green M, Choi JE, Gijón M, Kennedy PD, Johnson JK, Liao P, Lang X, Kryczek I, Sell A, Xia H, Zhou J, Li G, et al. CD8+ T cells regulate tumour ferroptosis during cancer immunotherapy. Nature. 2019; 569:270–74.
https://doi.org/10.1038/s41586-019-1170-y
PMID:31043744

32. Yang WS, Kim KJ, Gaschler MM, Patel M, Shchepinov MS, Stockwell BR. Peroxidation of polyunsaturated fatty acids by lipoxygenases drives ferroptosis. Proc Natl Acad Sci USA. 2016; 113:E4966–75.
https://doi.org/10.1073/pnas.1603244113
PMID:27506793

33. Gao M, Monian P, Pan Q, Zhang W, Xiang J, Jiang X. Ferroptosis is an autophagic cell death process. Cell Res. 2016; 26:1021–32.
https://doi.org/10.1038/cr.2016.95 PMID:27514700

34. Hassannia B, Vandenabeele P, Vanden Berghe T. Targeting Ferroptosis to Iron Out Cancer. Cancer Cell. 2019; 35:830–49.
https://doi.org/10.1016/j.ccell.2019.04.002
PMID:31105042

35. Jennis M, Kung CP, Basu S, Budina-Kolomets A, Leu JI, Khaku S, Scott JP, Cai KQ, Campbell MR, Porter DK, Wang X, Bell DA, Li X, et al. An African-specific polymorphism in the TP53 gene impairs p53 tumor suppressor function in a mouse model. Genes Dev. 2016; 30:918–30.

https://doi.org/10.1101/gad.275891.115
PMID:27034505

36. Müller S, Sindikubwabo F, Cañeque T, Lafon A, Versini A, Lombard B, Loew D, Wu TD, Ginestier C, Charafe-Jauffret E, Durand A, Vallot C, Baulande S, et al. CD44 regulates epigenetic plasticity by mediating iron endocytosis. Nat Chem. 2020; 12:929–38.
https://doi.org/10.1038/s41557-020-0513-5
PMID:32747755

37. Elgendy SM, Alyammahi SK, Alhamad DW, Abdin SM, Omar HA. Ferroptosis: An emerging approach for targeting cancer stem cells and drug resistance. Crit Rev Oncol Hematol. 2020; 155:103095.
https://doi.org/10.1016/j.critrevonc.2020.103095
PMID:32927333

38. Stockwell BR, Friedmann Angeli JP, Bayir H, Bush AI, Conrad M, Dixon SJ, Fulda S, Gascón S, Hatzios SK, Kagan VE, Noel K, Jiang X, Linkermann A, et al. Ferroptosis: A Regulated Cell Death Nexus Linking Metabolism, Redox Biology, and Disease. Cell. 2017; 171:273–85.
https://doi.org/10.1016/j.cell.2017.09.021
PMID:28985560

39. Di Nunno V, Frega G, Santoni M, Gatto L, Fiorentino M, Montironi R, Battelli N, Brandi G, Massari F. BAP1 in solid tumors. Future Oncol. 2019; 15:2151–62.
https://doi.org/10.2217/fon-2018-0915
PMID:31159579

40. Núñez MT, Hidalgo C. Noxious Iron-Calcium Connections in Neurodegeneration. Front Neurosci. 2019; 13:48.
https://doi.org/10.3389/fnins.2019.00048
PMID:30809110

41. Dodson M, Castro-Portuguez R, Zhang DD. NRF2 plays a critical role in mitigating lipid peroxidation and ferroptosis. Redox Biol. 2019; 23:101107.
https://doi.org/10.1016/j.redox.2019.101107
PMID:30692038

42. Liu LM, Xiong DD, Lin P, Yang H, Dang YW, Chen G. DNA topoisomerase 1 and 2A function as oncogenes in liver cancer and may be direct targets of nitidine chloride. Int J Oncol. 2018; 53:1897–912.
https://doi.org/10.3892/ijo.2018.4531
PMID:30132517
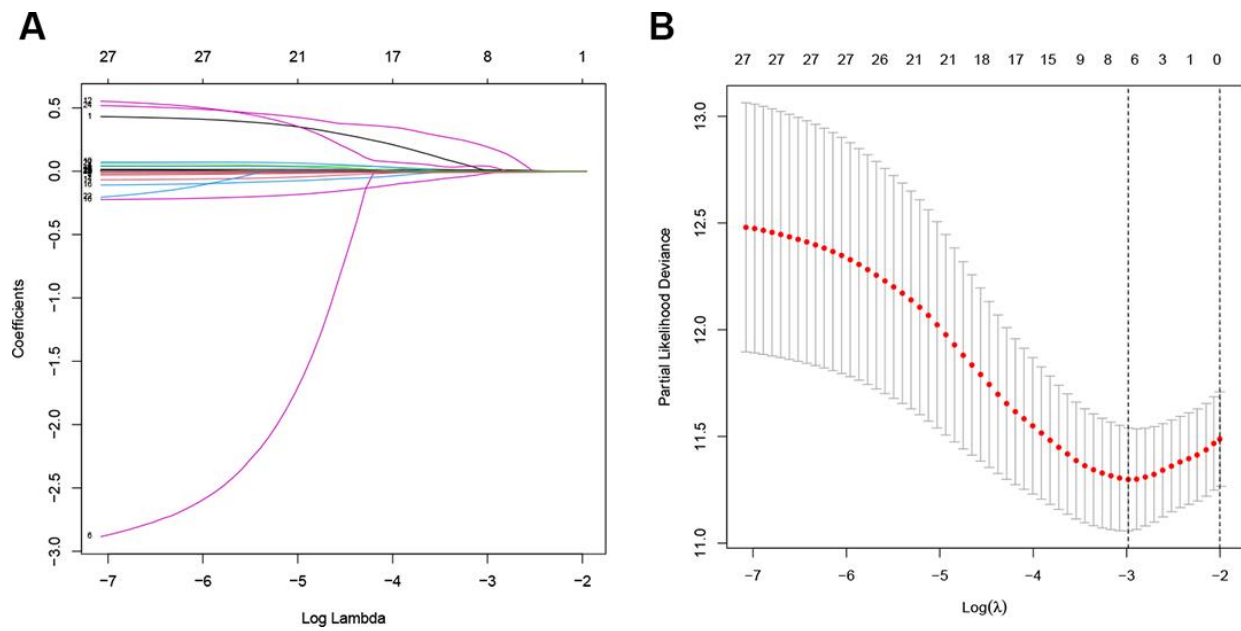
Supplementary Figure 1. LASSO regression analysis of 27 prognostic DEGs. (**A**) LASSO coefficient profiles of 27 genes. (**B**) Selection of the penalty parameter (λ).
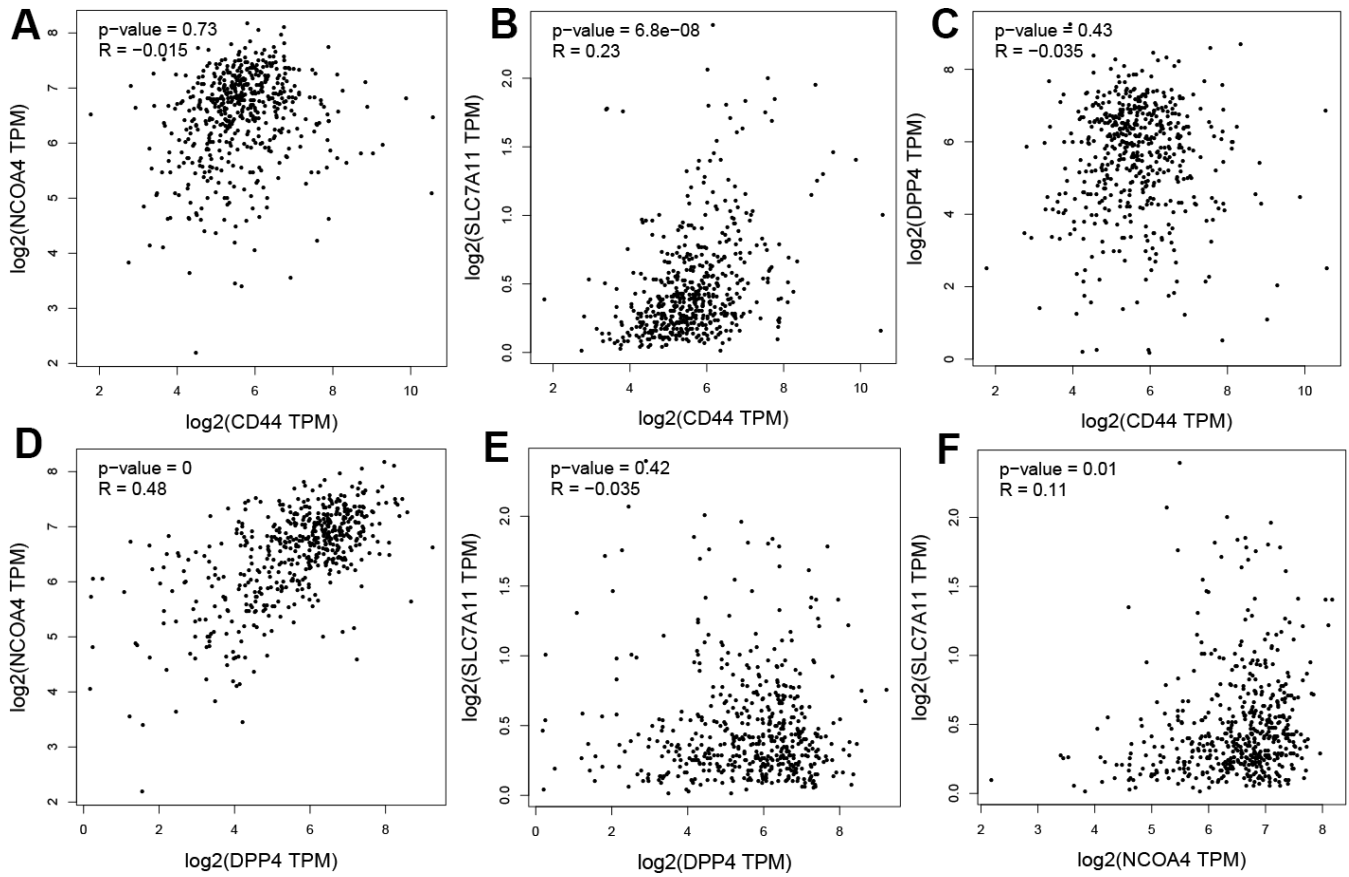
Supplementary Figure 2. (**A**–**F**) Co-expression analysis between four ferroptosis genes.
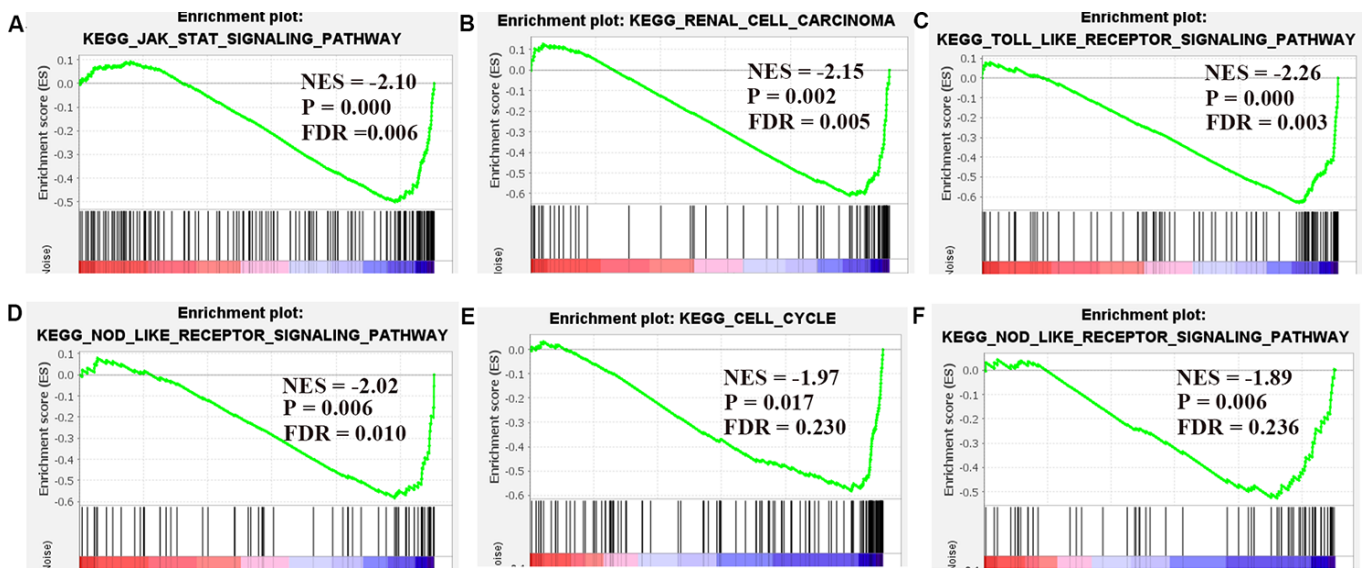
Supplementary Figure 3. (**A**–**F**) Enrichment curves for NCOA4 (**A**–**D**) and SLC7A11 (**E**, **F**) by GSEA analysis. NES, normalized enrichment score; FDR, false discovery rate.

Supplementary Tables

Supplementary Table 1. The list of the 64 ferroptosis-related genes from publications.

Ferroptosis-related genes	Name
ABCC1	ATP binding cassette subfamily C member 1
ACACA	Acetyl-CoA carboxylase alpha
ACO1	aconitase 1
ACSF2	acyl-CoA synthetase family member 2
ACSL3	acyl-CoA synthetase long-chain family member 3
ACSL4	acyl-CoA synthetase long-chain family member 4
AIFM2	apoptosis inducing factor mitochondria associated 2
AKR1C1	aldo-keto reductase family 1 member C1
AKR1C2	aldo-keto reductase family 1 member C2
AKR1C3	aldo-keto reductase family 1 member C3
ALOX12	arachidonate 12-lipoxygenase
ALOX15	arachidonate 15-lipoxygenase
ALOX5	arachidonate 5-lipoxygenase
ATP5MC3	ATP synthase membrane subunit c locus 3
BAP1	BRCA1 associated protein 1
CARS	cysteinyl tRNA synthetase
CBS	cystathionine beta synthase
CD44	CD44 molecule
CHAC1	ChaC glutathione- specific gamma-glutamyl cyclotransferase 1
CISD1	CDGSH iron sulfur domain 1
CRYAB	heat shock protein beta 5
CS	citrate synthase
DMT1	ferrous ion membrane transport protein DMT1
DPP4	dipeptidyl-dippeptidase-4
EMC2	ER membrane protein complex subunit 2
FADS2	fatty acid desaturase 2/acyl-CoA 6-desaturase
FANCD2	Fanconi anemia complementation group D2
FDFT1	farnesyl-diphosphate farnesyltransferase 1
FTH1	ferritin heavy chain 1
G6PD	glucose-6-phosphate dehydrogenase
GCLC	glutamate-cysteine ligase catalytic subunit
GCLM	glutamate-cysteine ligase modifier subunit
GLS2	glutaminase 2
GOT1	glutamic-oxaloacetic transaminase 1
GPX4	glutathione peroxidase 4
GSS	glutathione synthetase
HMGCR	3-hydroxy-3- methylglutaryl-CoA reductase
HMOX1	heme oxygenase 1
HSBP1	heat-shock 27-k Da protein 1
HSPB1	heat shock protein beta 1
IREB2	iron response element-binding protein 2
KEAP1	kelch-like ECH- associated protein 1
LPCAT3	lysophosphatidylcholine acyltransferase 3
MT1G	metallothionein-1G
NCOA4	nuclear receptor coactiva tor 4
NFE2L2	nuclear factor, erythroid 2 like 2

NFS1	cysteine desulfurase
NOX1	NADPH oxidase 1
NQO1	quinone oxidoreductase-1
PEBP1	phosphatidylethanolamine-binding protein 1
PGD	phosphoglycerate dehydrogenase
PHKG2	phosphorylase kinase ,g2
PTGS2	prostaglandin-endoperoxide synthase 2
RPL8	ribosomal protein L8
SAT1	spermidine/spermine N1-acetyltransferase 1
SLC1A5	solute carrier family 1 member 5
SLC7A11	solute carrier family 7 member 11
SQLE	squalene monooxygenase
STEAP3	six-transmembrane epithelial antigen of prostate 3
TFRC	transferrin receptor
TP53	tumor protein 53
VDAC2	voltage dependent anion channel 2
VDAC3	voltage dependent anion channel 3
ZEB1	zinc finger E-box-binding homeobox 1

Supplementary Table 2. Primers of 4 ferroptosis-related genes used in this study.

Genes	Primers (5'-3')
DPP4-F	TTCAGAACTATTCGGTCA
DPP4-R	ATAAAGATTCCTTCCTCCT
NCOA4-F	TCAACATAGAACGCACAT
NCOA4-R	AGAACTCCACCAATAGCA
SLC7A11-F	TATTCTATGTTGCGTCTCG
SLC7A11-R	TATCATTGTCAAAGGGTGC
CD44-F	CAGCTCATACCAGCCATCCA
CD44-R	GCTTGATGACCTCGTCCCAT
Actin-F	ACACTGTGCCCATCTACG
Actin-R	TGTCACGCACGATTTCC